Shape-Controlled Catalysts

DOI: 10.1002/anie.201002888

Enhancing by Weakening: Electrooxidation of Methanol on Pt_3Co and Pt Nanocubes**

Hongzhou Yang, Jun Zhang, Kai Sun, Shouzhong Zou, and Jiye Fang**

Direct methanol fuel cells (DMFCs) are attractive energy conversion devices for powering portable electronics by converting the chemical energy of methanol directly into electricity.[1–4] To increase the methanol oxidation activity and to reduce platinum loading, bimetallic catalysts of platinum alloyed with a less expensive metal M are often used.[5–10] Among different bimetallic catalysts, Pt/Ru has attracted most attention owing to its strong methanol oxidation enhancement. The improved catalytic activity is explained by the bifunctional mechanism[5] and the electronic effect.[6,7] In the bifunctional mechanism, the platinum sites are responsible for methanol oxidation to form adsorbed carbon monoxide (CO_{ads}), which poisons the catalyst surface for further fuel oxidation; the ruthenium sites provide adsorbed hydroxyl groups (OH_{ads}), which is the oxidant for the removal of CO_{ads}, at a much lower potential than on platinum. In the electronic effect, the presence of ruthenium changes the electronic structure of platinum in such a way that it lowers the CO adsorption energy. These two mechanisms often operate concurrently and are often invoked to explain the activity enhancement of other Pt/M alloys. Herein we present methanol oxidation on Pt_3Co nanocubes (NCbs), in which the enhanced methanol oxidation arises solely from the electronic effect.

It has been extensively shown that methanol oxidation is a structure-sensitive reaction on platinum surfaces. The dependence of catalytic activity on particle shape for methanol oxidation on Pt nanocrystals (NCs) has also been revealed.[11–14] These studies underscore the importance of surface structure through particle shape control when the activities of different catalysts are compared. Recently, we also developed a robust and general approach for synthesizing NCbs consisting of binary alloys of platinum and 3d transition metals, including Pt_3Co NCbs.[15] This approach provides a new avenue to compare methanol oxidation activity on structurally similar Pt_3Co and Pt NCbs, thus eliminating the activity difference arising from the surface structure effect. Pt/Co alloy nanoparticles (NPs) have been previously shown to possess a higher methanol oxidation activity compared to Pt NPs in both acidic and basic media.[8–10,16] To the best of our knowledge, this is the first comparative study of methanol oxidation on structurally controlled Pt and Pt alloy NCs.

Figure 1 a,e presents typical transmission electron microscopic (TEM) images of the Pt_3Co and Pt NCbs, showing a

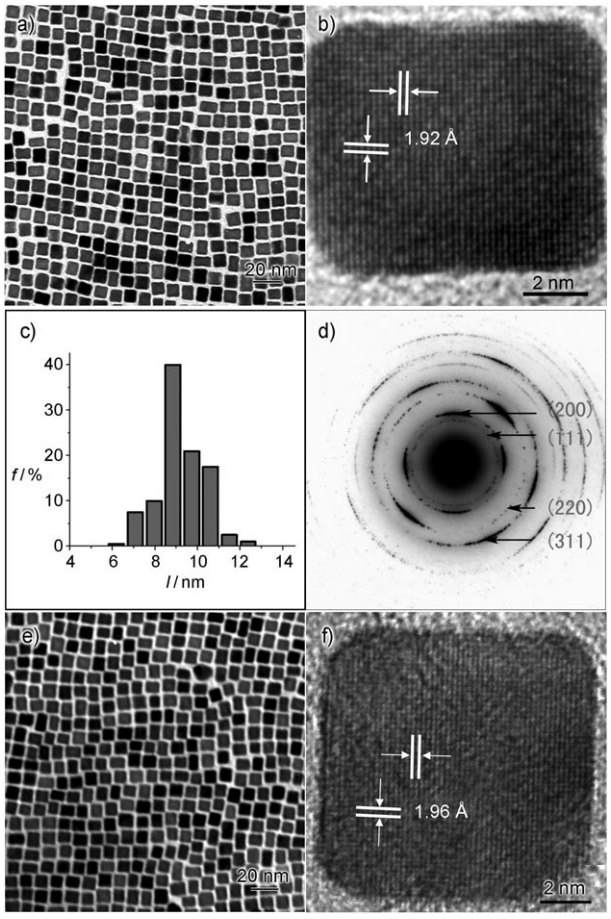

Figure 1. a) TEM image of Pt_3Co nanocubes (NCbs); b) HRTEM image of a single Pt_3Co NCb; c) size-distribution histogram (frequency *f* versus length *l*) of Pt_3Co NCbs determined using TEM image of about 200 NCs (equivalent side lengths were calculated based on the measured diagonals); d) SAED of Pt_3Co NCbs (ca. 300 NCs, negative pattern); e) TEM image of Pt NCbs; f) HRTEM image of a single Pt NCb.

[*] Dr. H. Yang, Prof. S. Zou
Department of Chemistry and Biochemistry
Miami University,Oxford, OH 45056 (USA)
E-mail: zous@muohio.edu
Dr. J. Zhang, Prof. J. Fang
Department of Chemistry
State University of New York at Binghamton
Binghamton, NY 13902 (USA)
E-mail: jfang@binghamton.edu
Homepage: http://chemiris.chem.binghamton.edu/FANG
Dr. K. Sun
Department of Materials Science and Engineering
University of Michigan
Ann Arbor, MI 48109 (USA)

[**] This work was supported by the NSF (DMR-0731382 and CHM-0616436), S^3IP, and Binghamton University.

Supporting information for this article is available on the WWW under http://dx.doi.org/10.1002/anie.201002888.

perfect morphology of nearly 100% NCbs (see also Supporting Information, Figure S1). Figure 1b,f shows high-resolution TEM (HRTEM) images of selected Pt_3Co and Pt NCbs, revealing highly crystalline cubes with clearly resolved lattice fringes. Because the measured *d* spacings (1.92 Å for Pt_3Co and 1.96 Å for Pt) are consistent with those of Pt_3Co (refer to JCPDS-ICDD card 29-0499) and Pt (refer to JCPDS-ICDD card 04-0802) {200} lattice planes, these images not only demonstrate that both the Pt_3Co and Pt NCbs are perfect {100}-orientated structures, but also indirectly verify the composition of Pt_3Co. Moreover, no crystal-core distortion was determined from both HRTEM images. Figure 1c illustrates a size-distribution histogram of this Pt_3Co sample based on a measurement of about 200 selected NCbs in a TEM image. The average side-length of these selected Pt_3Co NCbs was about (9.2 ± 0.8) nm, while that for Pt NCbs was about (9.0 ± 0.5) nm (not shown).[17] ICP-MS analysis suggests that the molar ratio between Pt and Co in this Pt_3Co sample is around 3.02:1.00, which is in good agreement with the average result from energy-dispersive X-ray spectroscopic (EDS) evaluation (ca. 76.8:23.2; Supporting Information, Figure S2). Further support for 3:1 Pt/Co molar ratio can be found in X-ray diffraction (XRD) patterns (see below). Furthermore, using both ICP-MS and EDS, no tungsten could be detected in both the Pt_3Co and Pt NCbs. As depicted in Figure 1d, a negative-image SAED pattern taken from about 300 Pt_3Co NCbs exhibits four-fold symmetry in the ring corresponding to the (200) plane, indicating that the NC arrays are (100)-textured. This conclusion is also supported by the observations that the (111) diffraction ring is very weak and the (222) ring is absent in Figure 1d.

To further verify the structure of these NCbs, XRD patterns of both the Pt_3Co and Pt samples are presented in the Supporting Information, Figure S3. By indexing these XRD patterns using the above-mentioned standard ICDD PDF cards, we confirmed that the as-synthesized NCs possess highly crystalline fcc Pt_3Co or Pt phases with the $Fm3m$ (Figure S3a,b) and $Fm\bar{3}m$ space groups (Figure S3c,d), respectively. As reported previously,[15,18,19] the strongly enhanced (200) peaks of Pt_3Co (Figure S3a) and Pt NCbs (Figure S3c) overpower the intensities from all other diffraction peaks detected (Figure S3b,d), indicating that the assembled Pt_3Co and Pt NCbs align perfectly flat on the polished surface of silicon wafer with (100) texture. This information further supports the conclusion that the Pt_3Co and Pt NCbs have a {100}-dominated cubic morphology and a very narrow shape distribution.

As discussed previously,[15] the shape of Pt_3Co evolved in a solution system is determined synergically by a nucleation step and subsequent Ostwald-ripening growth on the existing seeds (or nuclei). The platinum precursor–tungsten system formed by introduction of $[W(CO)_6]$ acts as a "buffer", ensuring steady growth of alloy particles with a sufficient feedstock during the nucleation stage, whereas the use of a mixed solvent/capping agent, oleylamine and oleic acid in a fixed volume ratio of about 4:1, is equally significant in the control of crystal growth into a {100}-terminated NCbs.

Before electrochemical measurements were made, the glassy carbon (GC) electrode supported catalysts were subjected to argon plasma treatment and potential cycling between 0.05 and 1.0 V to remove residual organic solvent and surfactant and to further clean the particle surface. These treatments have no apparent effect on the particle morphology as revealed by EM images (Supporting Information, Figures S4,S5). Furthermore, a cobalt dissolution current was absent on Pt_3Co cubes, in contrast to the Pt/Co alloys prepared by sputtering.[20] Typical cyclic voltammograms (CVs) of Pt_3Co and Pt NCbs recorded in deaerated 0.1 M $HClO_4$ are shown in Figure 2a. For Pt_3Co NCbs, the main

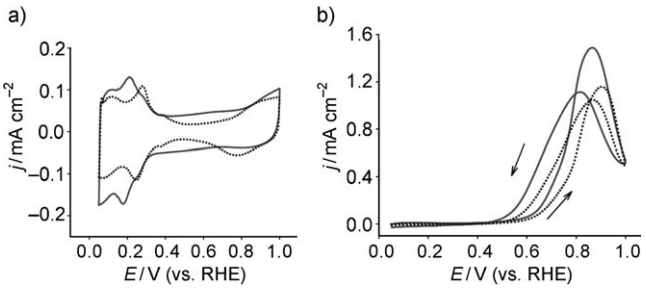

Figure 2. a) Cyclic voltammograms of Pt_3Co (——) and Pt NCbs (•••••) in 0.1 M $HClO_4$ (scan rate 0.1 $V s^{-1}$); b) cyclic voltammograms of methanol oxidation on Pt_3Co (——) and Pt NCbs (•••••) in 0.1 M $HClO_4$ + 1 M MeOH (scan rate 0.02 $V s^{-1}$). Arrows indicate the potential scan direction.

feature of the voltammogram from 0.05 to 0.35 V is a pair of peaks at about 0.20 V together with a pair of weak peaks at 0.30 V. These current features can be attributed to hydrogen adsorption/desorption on Pt(100) surface sites, suggesting the particle surface is clean. Compared to the Pt NCbs, these peaks shift negatively by nearly 80 mV, suggesting weaker hydrogen adsorption on Pt_3Co particle surfaces.[11] At the more positive potentials, an oxidative current from the formation of surface oxides appears at 0.80 V. Correspondingly, a very weak surface oxide reduction peak is discernable in the reverse potential scan. The surface oxidation onset potential of Pt_3Co NCbs is significantly more positive than that of Pt NCbs, indicating that Pt_3Co NCbs are more difficult to oxidize. This assertion is also supported by the much smaller oxide reduction current observed on Pt_3Co NCbs compared to Pt NCbs. The less surface oxidation and the weaker hydrogen adsorption arise from the decrease of platinum d-band center by alloying with cobalt, as predicted by the d-band theory[21] and demonstrated experimentally by XPS.[20] The decrease of the platinum d-band center lowers the adsorption energy of adsorbates and will therefore affect its catalytic activity. For comparison with literature results, we recorded CVs in 0.5 M H_2SO_4 as well. The CV of Pt NCbs after the plasma and potential cycling treatments is similar to that reported by Feliu et al.[22] The voltammetric differences between Pt_3Co and Pt NCbs seen in 0.1 M $HClO_4$ are also observed in 0.5 M H_2SO_4 (Supporting Information, Figure S6). This comparison further suggests that the above-mentioned cleaning treatments have little effect on the particle structure.

Figure 2b shows the voltammograms of methanol oxidation on Pt_3Co and Pt NCbs recorded in 0.1 M $HClO_4$ + 1 M MeOH. At potentials below 0.60 V, the oxidation current is

negligible in both voltammograms because the active sites are poisoned by CO_{ads}, an intermediate from dehydrogenation of methanol. At more positive potentials, the oxidation current takes off rapidly, signifying that significant methanol oxidation occurs. The oxidation current peaks at 0.87 V on Pt_3Co NCbs, which is about 30 mV more negative than that on Pt NCbs. The overall current density on the positive potential sweep is higher on Pt_3Co NCbs. In the reversed potential scan, the current peak appears at 0.82 V on Pt_3Co and 0.87 V on Pt NCbs. The current density is higher on Pt_3Co NCbs at potentials lower than 0.85 V until about 0.45 V, where the oxidation current is again negligible because of the surface poisoning. The higher current density on Pt_3Co NCbs at lower potentials indicates enhanced methanol oxidation catalytic activity. This observation agrees with those reported on Pt/Co alloy particles.[9,10,23,24] The advantage of present study is that the particle shape and hence the catalyst surface structure is controlled. Therefore, the enhancement in catalytic activity is solely from the alloying effect, as opposed to the possible additional structural effect in the previous studies.

To evaluate the steady-state catalytic activity, chronoamperometric (CA) measurements were performed at 0.50, 0.60, and 0.70 V. The current transient was recorded after the electrode potential was stepped from 0.05 V to the desired potentials. The current–time response at 0.60 V is similar to that at 0.70 V, except for a smaller current at the lower potential; therefore, only results recorded at 0.50 and 0.70 V are presented in Figure 3. Consistent with the CV results, the

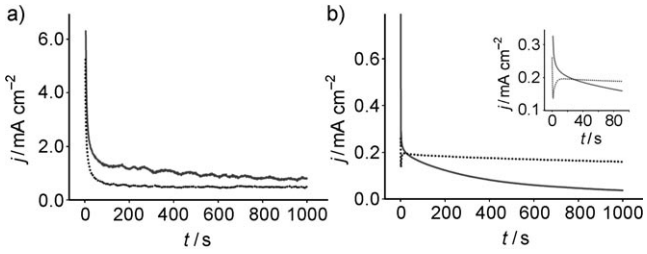

Figure 3. Chronoamperometric plots of MeOH oxidation at a) 0.50 V and b) 0.70 V on cubic Pt_3Co (——) and Pt NCbs (•••••) in 0.1 M $HClO_4$ + 1 M MeOH. The inset in (b) is an enlargement of a shorter time section. Initial potential: 0.05 V.

methanol oxidation current density (normalized to platinum surface area) of Pt_3Co NCbs is higher than that of Pt NCbs at 0.50 V over the entire time period examined. Interestingly, at 0.70 V, the current density on Pt_3Co NCbs is initially higher, but decays rapidly. After about 30 s, it becomes lower than that on Pt NCbs (Figure 3b, inset). From this point on, the current density on Pt NCbs decays slowly, but continues to rapidly decrease on Pt_3Co NCbs. By the end of the measurement, the methanol oxidation current density on Pt NCbs is more than four times of that on Pt_3Co NCbs.

We then attempted to understand the enhanced methanol oxidation on Pt_3Co NCbs. It is generally accepted that electrochemical oxidation of methanol on platinum catalysts follows a "dual-pathway" mechanism.[25–30] In the direct pathway, methanol oxidation produces intermediates that are dissolved in the solution and are oxidized to form CO_2. In the indirect pathway, the oxidation goes through the formation of CO_{ads}, which poisons the catalyst surface. A frequently invoked explanation of enhanced methanol oxidation on Pt/Co alloys is the facilitation of CO oxidation by forming OH_{ads} at lower potentials in the presence of cobalt,[23] similar to that used in Pt/Ru system. This is apparently not the case in the present study, as our CO stripping experiments clearly show that Pt_3Co NCbs are less effective for CO removal (Supporting Information, Figure S7), which is very likely due to the lack of OH_{ads} necessary for CO oxidation. The formation of OH_{ads} on Pt_3Co NCbs requires a much higher potential compared to that on Pt NCbs, as evident in the formation of surface oxides at a much higher potential on the former particles. The less-facile CO removal on Pt_3Co NCbs is responsible for the rapid decay of methanol oxidation observed at 0.70 V. In contrast, on Pt NCbs CO oxidation already takes place at 0.70 V, therefore there is not much CO accumulation on the surface and methanol oxidation proceeds at nearly the same rate. This argument is in accordance with the CV results of methanol oxidation. On the timescale of CV measurements, CO poisoning of the Pt_3Co NCb surface is not severe and therefore a higher methanol oxidation current was observed on Pt_3Co NCbs. The higher activity of Pt_3Co NCbs for methanol oxidation at 0.50 V, where CO oxidation does not occur on either particles, further supports the proposal that facile CO oxidation is not responsible for the observed enhanced methanol oxidation. This leaves two possibilities: CO coverage on Pt_3Co NCbs is lower than that on Pt NCbs, and/or the indirect pathway is promoted by Pt_3Co NCbs. By using dilute CO solutions to form CO_{ads}, it is possible to monitor the rate of CO adsorption by measuring the amount of CO_{ads} formed at a given time.[31] Our results reveal that CO coverage on Pt_3Co NCbs is about 50% of that on Pt NCbs when a 100-fold diluted CO saturated solution was used for forming CO adlayer in 2 min. This observation agrees with that reported by Uchida et al., namely that CO adsorption is much slower on PtCo alloy surfaces.[31] The slower CO adsorption delays surface blocking and leads to a higher methanol oxidation activity at a short time, which is in agreement with the experimental observations (Figure 3). It has been demonstrated by Cao et al. that direct pathway on Pt(100) surface is not as important as on the other two low-index planes.[32]

In summary, we have successfully prepared high-quality and {100}-facet-terminated Pt_3Co and Pt NCbs. A comparative study on their electrocatalytic activities towards methanol oxidation shows that Pt_3Co NCbs are much more active. The enhanced catalytic activity is attributed to weaker and slower CO adsorption. This work suggests that the Pt_3Co NCbs could be promising anode electrocatalysts for direct methanol fuel cells with high activity, low cost, and CO poisoning resistance.

Experimental Section

Cobalt(II) acetate tetrahydrate (99.999%), tungsten hexacarbonyl (99.9%), oleic acid (90%), and oleylamine (70%) were obtained from Sigma–Aldrich. Platinum(II) acetylacetonate (49.3–49.8% Pt),

absolute ethanol, and anhydrous hexanes (98.5%) were purchased from Gelest, Alfa Aesar, AAPER, and BDH, respectively. Perchloric acid ($HClO_4$, 70%, double distilled) and sulfuric acid (H_2SO_4, 95.0–98.0%, double distilled) were obtained from GFS chemicals, and methanol is from Pharmco. All chemicals were used without further purification. Nanocube synthesis and characterization are described in detail in the Supporting Information.

Received: May 13, 2010
Published online: August 16, 2010

Keywords: electrocatalysis · fuel cells · methanol oxidation · nanocubes · platinum

[1] B. C. H. Steele, A. Heinzel, *Nature* **2001**, *414*, 345 – 352.
[2] M. S. Dresselhaus, I. L. Thomas, *Nature* **2001**, *414*, 332 – 337.
[3] M. Winter, R. J. Brodd, *Chem. Rev.* **2004**, *104*, 4245 – 4270.
[4] W. Vielstich, A. Lamm, H. A. Gasteiger, *Handbook of Fuel Cells: Fundamentals, Technology, Applications*, Wiley, New York, **2003**.
[5] M. Watanabe, S. Motoos, *J. Electroanal. Chem.* **1975**, *60*, 267 – 273.
[6] M. Krausa, W. Vielstich, *J. Electroanal. Chem.* **1995**, *379*, 307 – 314.
[7] Y. Tong, H. S. Kim, P. K. Babu, P. Waszczuk, A. Wieckowski, E. Oldfield, *J. Am. Chem. Soc.* **2002**, *124*, 468 – 473.
[8] E. Antolini, J. R. C. Salgado, E. R. Gonzalez, *Appl. Catal. B* **2006**, *63*, 137 – 149.
[9] Q.-S. Chen, S.-G. Sun, Z.-Y. Zhou, Y.-X. Chen, S.-B. Deng, *Phys. Chem. Chem. Phys.* **2008**, *10*, 3645 – 3654.
[10] G. Chen, D. Xia, Z. Nie, Z. Wang, L. Wang, L. Zhang, J. Zhang, *Chem. Mater.* **2007**, *19*, 1840 – 1844.
[11] J. Solla-Gullòn, F. J. Vidal-Iglesias, A. Lòpez-Cudero, E. Garnier, J. M. Feliu, A. Aldaz, *Phys. Chem. Chem. Phys.* **2008**, *10*, 3689 – 3698.
[12] N. Tian, Z.-Y. Zhou, S.-G. Sun, Y. Ding, Z. L. Wang, *Science* **2007**, *316*, 732 – 735.
[13] S. S. Kim, C. Kim, H. Lee, *Top. Catal.* **2010**, *53*, 686 – 693.
[14] X. Teng, H. Yang, *Front. Chem. Eng. China* **2010**, *4*, 45 – 51.
[15] J. Zhang, J. Fang, *J. Am. Chem. Soc.* **2009**, *131*, 18543 – 18547.
[16] L. Liu, E. Pippel, R. Scholz, U. Gsele, *Nano Lett.* **2009**, *9*, 4352 – 4358.
[17] To minimize the statistical error, a diagonal of each projected image was measured and its equivalent side length was subsequently calculated based on an assumption that the projection image of each NC is exactly square.
[18] C. Wang, H. Daimon, Y. Lee, J. Kim, S. Sun, *J. Am. Chem. Soc.* **2007**, *129*, 6974 – 6975.
[19] W. Lu, J. Fang, K. L. Stokes, J. Lin, *J. Am. Chem. Soc.* **2004**, *126*, 11798 – 11799.
[20] M. Wakisaka, S. Mitsui, Y. Hirose, K. Kawashima, H. Uchida, M. Watanabe, *J. Phys. Chem. B* **2006**, *110*, 23489 – 23496.
[21] J. R. Kitchin, J. K. Nørskov, M. A. Barteau, J. G. Chen, *Phys. Rev. Lett.* **2004**, *93*, 156801.
[22] J. Solla-Gullón, P. Rodríguez, E. Herrero, A. Aldaz, J. M. Feliu, *Phys. Chem. Chem. Phys.* **2008**, *10*, 1359 – 1373.
[23] J. Zeng, J. Y. Lee, *J. Power Sources* **2005**, *140*, 268 – 273.
[24] X. Zhang, K.-Y. Chan, *J. Mater. Chem.* **2002**, *12*, 1203 – 1206.
[25] M. Z. Markarian, M. E. Harakeh, L. I. Halaoui, *J. Phys. Chem. B* **2005**, *109*, 11616 – 11621.
[26] T. H. M. Housmans, A. H. Wonders, M. T. M. Koper, *J. Phys. Chem. B* **2006**, *110*, 10021 – 10031.
[27] C. Korzeniewski, C. L. Childers, *J. Phys. Chem. B* **1998**, *102*, 489 – 492.
[28] Y. X. Chen, A. Miki, S. Ye, H. Sakai, M. Osawa, *J. Am. Chem. Soc.* **2003**, *125*, 3680 – 3681.
[29] E. A. Batista, G. R. P. Malpass, A. J. Motheo, T. Iwasita, *Electrochem. Commun.* **2003**, *5*, 843 – 846.
[30] H. Wang, T. Löffler, H. Baltruschat, *J. Appl. Electrochem.* **2001**, *31*, 759 – 765.
[31] H. Uchida, K. Izumi, K. Aoki, M. Watanabe, *Phys. Chem. Chem. Phys.* **2009**, *11*, 1771 – 1779.
[32] D. Cao, G.-Q. Lu, A. Wieckowski, S. A. Wasileski, M. Neurock, *J. Phys. Chem. B* **2005**, *109*, 11622 – 11633.

